

---

# The Canadian Cropland Dataset: A New Land Cover Dataset for Multitemporal Deep Learning Classification in Agriculture

---

Amanda A. Boatswain Jacques<sup>1,2</sup>, Abdoulaye Baniré Diallo<sup>1</sup>, Etienne Lord<sup>2</sup>

<sup>1</sup> Département d'informatique, Laboratoire d'algèbre,  
de combinatoire et d'informatique mathématique (LACIM)

Université du Québec à Montréal  
PO BOX 8888 Downtown Station, H3C 3P8

<sup>2</sup> Agriculture and Agri-Food Canada  
430 Gouin Boulevard, Saint-Jean-sur-Richelieu, J3B 3E6  
boatswain\_jacques.amanda@courrier.uqam.ca

## Abstract

Monitoring land cover using remote sensing is vital for studying environmental changes and ensuring global food security through crop yield forecasting. Specifically, multitemporal remote sensing imagery provides relevant information about the dynamics of a scene, which has proven to lead to better land cover classification results. Nevertheless, few studies have benefited such high spatial and temporal resolution data due to the difficulty of accessing reliable, fine-grained and high-quality annotated samples to support their hypotheses. Therefore, we introduce a temporal patch-based dataset of Canadian croplands, enriched with labels retrieved from the *Canadian Annual Crop Inventory*. The dataset contains 78,536 manually verified and curated high-resolution (10 m/pixel, 640 x 640 m) geo-referenced images from 10 crop classes collected over four crop production years (2017-2020) and five months (June-October). Each instance contains 12 spectral bands, a RGB image, and additional bands corresponding to commonly used vegetation indices. Individually, each category contains at least 4,800 images. Moreover, as a benchmark, we provide models and source code that allow a user to predict the crop class using a single image (ResNet, DenseNet, EfficientNet) or a sequence of images (LRCN, 3D-CNN) from the same location. In perspective, we expect this evolving dataset to propel the creation of robust agro-environmental models that can accelerate the comprehension of complex agricultural regions by providing accurate and continuous monitoring of land cover.

**Keywords:** satellite imagery, remote sensing, dataset, agriculture, cropland, supervised learning, image classification, deep learning.

## 1 Introduction

The term *land cover*, defined as the surface cover on the ground, comprises anything including vegetation, urban development, mountains or others. Whereas land cover corresponds to a physical property of the ground, *land use* refers to the function or purpose attributed to a piece of land.



Figure 1: An image mosaic of RGB images taken from the 2019 data of the *Canadian Cropland Dataset*. The dataset contains Sentinel-2 images of North American crops over 5 distinct seasonal periods (June to October). The dimensions of each image are 640 m × 640 m (64 × 64 pixels).

28 These functions fall within various categories such as recreation, agriculture, lodging, business or  
 29 governmental. The ability to accurately map, delineate and characterize land cover provides essential  
 30 information which can improve resource management, activity planning and change detection [28].  
 31 Monitoring the land cover and land use changes in perennial, annual and cover crops can help  
 32 agronomists and agricultural agencies to improve management and address issues related to climate  
 33 change, global food security and biodiversity [26, 19]. This is done through the analyses of remote  
 34 sensing (RS) data obtained via instruments such as satellites in orbit, or with proximal sensing using  
 35 unmanned aerial vehicles (UAV) like drones, which generate data with very high spatial resolution  
 36 [9, 42, 44].

37 Significant advances in DL are still required to develop models capable of tackling real RS problems at  
 38 a global scale with high reliability and repeatability [14, 9, 35]. We provide a valuable resource to help  
 39 close this gap by presenting the *Canadian Cropland Dataset* (Figure 1). In sum, **our contributions**  
 40 are the following: (1) a collection of image patches of Canadian agricultural croplands containing  
 41 over 75,000 unique instances retrieved from the *Sentinel-2* satellite constellation, (2) a RS dataset that  
 42 can be used in both temporal studies and in fixed-time analyses, and finally (3) an evaluation of the  
 43 performance of agricultural land classification using a dynamic *Long-Term Recurrent Convolutional*  
 44 *Network* (LRCN) and 3D-CNN network architectures against more traditional static image analysis  
 45 architectures such as the ResNet, DenseNet and EfficientNet.

## 46 2 Related Work

47 Supervised classification of land cover is one of the most prominent active research areas in RS  
 48 hyperspectral image analysis [44, 9, 39, 35]. Early pioneering studies have explored the use of  
 49 handcrafted features constructed using algorithms to differentiate between scenes and land cover  
 50 types [16, 3, 42], while others have incorporated texture information and/or ancillary data [19, 9].  
 51 More recent studies have explored DL architectures in higher level (i.e. pixel-level) classification of  
 52 land cover [24] and the automatic delineation of land cover boundaries (*i.e.* semantic segmentation)  
 53 [25]. Deep Neural Networks (DNN) infer high-level hierarchical features that describe the complex  
 54 non-linear relationships that exist between the spectral information of satellite imagery and the  
 55 observed material or scene [9]. When sufficient data is available, these networks can perform well  
 56 even in the presence of noisy data [17]. Several examples of DL applications include work by  
 57 Song *et al.* [34], who used a Convolutional Neural Network (CNN) to classify land cover with  
 58 medium-resolution (30 m) imagery from the *Landsat-8* satellite. This CNN outperformed other  
 59 methods such as an SVM and an RF, but had a low average overall accuracy falling below 67% for  
 60 all models. Another work by Masoud *et al.* [25] developed a Multiple-Dilation Fully Convolutional  
 61 Network (MD-FCN) to classify agricultural field boundaries in imagery retrieved from Sentinel-2.

62 The FCN performed semantic segmentation (pixel-wise image classification) while the addition  
63 of dilated kernels preserved resolution without adding parameters to be learned. Although lower  
64 resolution boundaries were fragmented or missing, general boundaries were properly labeled.

65 The emergence of modern satellite sensors, such as Sentinel-2, has generated a wealth of rich  
66 spectral data with both high temporal resolution (a few days between measurements) and high spatial  
67 resolution (from 10 m/pixel) at a low cost. Consequently, the temporal parameter can now be exploited  
68 as a new dimension in analyses to compare pairs of images or time series when performing land cover  
69 classification [9, 5, 19]. Several examples of studies using multitemporal data include work by Mazzia  
70 *et al.* [26], who developed a pixel-recurrent CNN to classify pixels within 15 types of agricultural  
71 crops. Their proposed model exploited traits such as time correlation, temporal pattern extraction  
72 and multi-class classification modules, and provided very high classification accuracies (above 90%)  
73 compared to other baseline models. Kussul *et al.* [22] developed a 2D-CNN to perform patch-based  
74 classification ( $7 \times 7$  pixels) of land cover in Ukraine using a combined dataset of Landsat-8 and  
75 Sentinel-1 imagery at four different time periods in the growth season. The 2D-CNN differentiated  
76 between 11 classes (8 corresponding to major agricultural crops) with very high accuracy (94.6%).  
77 More recently, Campos-Taberner *et al.* [6] investigated the use of a Bi-Long Short-Term Memory (Bi-  
78 LSTM) network using pixel-based Normalized Difference Vegetation Index or NDVI (see Appendix  
79 A.3: *Definition of Vegetation Indices*) data provided by Sentinel-2 to follow the phenology and  
80 classification of 16 major crop types in Spain. They obtained high-precision levels between 92.9% to  
81 99.9%. In another study [43], a pixel-based 1D-CNN, an LSTM, a Gated-Recurrent Units (GRU), an  
82 LSTM-CNN, and a GRU-CNN model were used to classify 7 crop types in China with incomplete  
83 Sentinel-2 imagery (only 10 bands). Even with 43.5% missing data, their classifiers achieved an  
84 accuracy between 81.21% and 86.57%.

85 Some noticeable RS datasets closest to our work are the recently created *BigEarthNet-MM* [35],  
86 *Eurosat* [14], *CropHarvest* [38], *Calcrop21* [10] and *Denethor* [20] datasets. The *BigEarthNet-MM*  
87 [35] is a multimodal, multi-label dataset containing 590,326 pairs of Sentinel-1 and Sentinel-2 image  
88 patches collected since June 2017. It currently features 12 Sentinel-2 spectral bands as TIFF images  
89 with dimensions of  $120 \times 120$  pixels ( $1,200 \times 1,200$  m, for the 10 m bands) collected in 10 European  
90 countries (Austria, Belgium, Finland, Ireland, Kosovo, Lithuania, Luxembourg, Portugal, Serbia,  
91 Switzerland). This dataset was manually validated through visual inspection and was annotated using  
92 the CORINE land cover map of 2018 with 43 classes of land cover, including agricultural classes  
93 such as rice fields, vineyards, fruit trees and berry plantations, olive groves, pastures, annual crops  
94 associated with permanent crop, complex cultivation patterns, and agro-forestry areas. Alternatively,  
95 the *Eurosat* dataset contains a total of 27,000 land use images in 10 classes and is also noteworthy  
96 for its high-spectral resolution (12 bands per image, Sentinel-2) but lacks in the granularity of the  
97 crop classes (annual crop, permanent crop, pasture). Although some of these datasets ([38, 20, 10])  
98 are similar in the number of major crop categories (at least 9), our dataset is unique due to its large  
99 geographical area and high spatio-temporal information (more than 2 years) on top of the Sentinel  
100 bands. Moreover, 70% of geolocations have an image collection of at least 10 images (over 4 years),  
101 allowing a temporally rich monitoring of a field through a multi-year, multi-crop rotation.

### 102 3 Dataset creation

103 The *Canadian Cropland Dataset* can be directly downloaded from our github repository<sup>1</sup>, along with  
104 the code and models presented in this paper. The dataset is released under the *Montreal Data License*  
105 (see Appendix A.8) and a specific *Datasheet for Datasets* can be found in Appendix A.9.

106 **Collection of satellite imagery** The images in the dataset originate from the *Sentinel-2* constellation,  
107 which comprises two satellites (Sentinel-2A and 2B) that share the same sun-synchronous orbit phased  
108 at 180 degrees to each other. On average, the constellation takes a complete image of the Earth every  
109 5 days, creating a collection of roughly 18 registered images per month for the region of Canada

<sup>1</sup><https://github.com/bioinfoUQAM/Canadian-cropland-dataset>

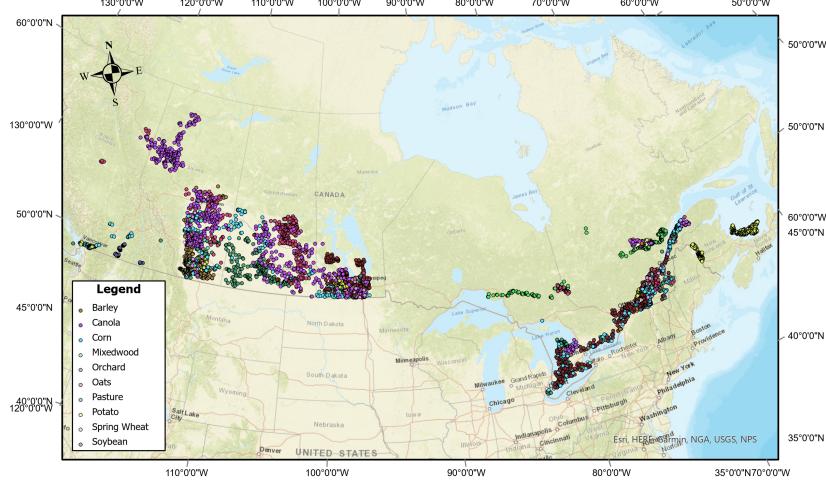


Figure 2: Map representing an overview of the selected geographical locations used in the *Canadian Cropland Dataset*. Markers are randomly chosen fields and are color-coded by the 2019 crop types. The map was created using ArcGis Pro 2.8.0 (<https://esri.com/en-us/arcgis/>).

[37]. Google Earth Engine (GEE) was selected as the main image manipulation platform due to its easy access to large records of satellite data, ancillary data, processing algorithms and free cloud computing resources and [12, 21]. Images with a cloud cover percentage above 5% were rejected, and we applied a final bitwise operation on the "cloud mask" band Q60 to remove any remnant cloud or shadow pixels. Following this, a median image for each month was produced by calculating the median of the values across all pixels and spectral bands in a collection. Median images of croplands at five different periods in the growth season (June, July, August, September and October) were retrieved. Each image is composed of 12 spectral bands which range from the Visible (VNIR) and Near Infra-Red (NIR) to the Short Wave Infra-Red (SWIR) wavelengths [37]. All the bands and their descriptions are listed in Table A.1 of the Appendix section. Finally, a region of  $64 \times 64$  pixels centered on each field between the years 2017 to 2020 was extracted and downloaded directly from GEE, giving rise to a rich multi-year dataset with unique long-term crop rotation patterns.

**Selection of geographical points** To label each image, we used the *Canadian Annual Crop Inventory* (ACI) developed by Agriculture and Agri-Food Canada (AAFC) and distributed using an *Open Government License*. The overall accuracy of the crop inventory is at least 90.56% at a final spatial resolution of 30 m. Table 3 (Appendix A.2) provides a summary of the regional crop class accuracies. Locations were selected randomly from 10 predominant North American crops with layers available in the ACI: barley (*Hordeum vulgare*), canola (*Brassica napus*), corn (*Zea mays*), mixedwood, oat (*Avena sativa*), orchard crops, pasture, potatoes(*Solanum tuberosum*), soybeans (*Glycine max*(L.) Merr.) and spring wheat (*Triticum aestivum* (L.). A total of 6,633 geographical points were manually validated by overlapping the 2019 crop type mask with each Sentinel-2 median image. Figure 2 shows the entire study region considered, as well as the classes of the selected points.

**Creation of vegetation indices** Vegetation indices quantify traits such as the amount of biomass, the vigor or the growth dynamics present in a spectral image [40, 41]. Using the original Sentinel-2 bands, we derived additional bands for 5 common vegetation indices (see Appendix A.3 for mathematical definitions). These image transformations were applied directly on the GEE cloud computing platform. After gathering the additional vegetation index bands, a composite image was generated by duplicating the information across 3 channels and saving them as .png files for ease of use with deep learning frameworks. For example, the created images are compatible with a ResNet architecture. An RGB dataset was also created by combining the visible red, green and blue bands (identified as the Sentinel-2 bands: B4, B3, B2) in a single image (see Figure A.4 in Appendix).

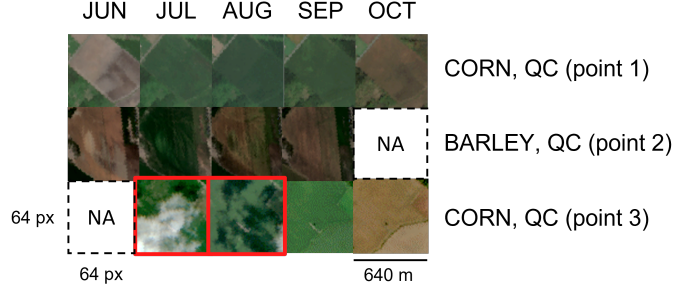


Figure 3: Examples of collected images for three locations (point 1 to 3). At the right side of the figure, supplementary information are shown including the crop class and province acronym. An example of removed images due to the presence of clouds are indicated by a red outline and missing images by *NA*. The image dimension is 64 pixels (px) corresponding to 640 m for each side.

141 **Data cleaning** The data were curated using visual observation to exclude any low quality image  
 142 that contained satellite artifacts or cloud pixels missed by the previously applied filters (see section  
 143 3: *Collection of satellite imagery*). The cleaning process was done using the RGB images and the  
 144 tagging of improper images was performed by 2 trained individuals. For each geographical location,  
 145 the raw data is supplied to the user in the form of a .zip file with all the original Sentinel-2 bands and  
 146 composite bands.

147 **Training, Validation and Test sets** The dataset comes prepackaged in dedicated training (70%),  
 148 validation (15%) and testing sets (15%) suitable for use with Keras or Tensorflow image data  
 149 generators. These sets remain the same for each individual year and image type (i.e NDVI, PSRI,  
 150 etc.). Images belonging to the same geographical coordinates were kept together during the dataset  
 151 splitting process to reduce overfitting.

## 152 4 Dataset analysis

153 **Dataset image distribution** Analyses were performed to calculate the number of images originating  
 154 from each time period (year, month), crop types and provinces. A total of 46 crop classes were  
 155 initially observed from the crop rotation patterns. The final version of the dataset targets the 10  
 156 most common crops that were present in Canada over the study period (Figure 4). The final image  
 157 counts for each category are: barley: 5,382; canola: 11,366; corn: 12,878; mixedwood: 4,981; oats:  
 158 4,807; orchards: 6,594; pasture and forages: 8,797; potatoes: 5,294; soybean: 10,208; spring wheat:  
 159 8,229. Additional figures and full statistics on the dataset can be consulted in the supplementary  
 160 material. Roughly 88.2 % of all points have 3 or more images available for each growth season.  
 161 However, looking at the monthly analyses, images from the month of June were less common overall.  
 162 This may be due to the high percentage of cloud cover that is associated with the spring season  
 163 in Canada and that was observed within the dataset (*data not shown*). To mitigate this, missing  
 164 data could be retrieved using a multi-source data fusion approach by gathering images from another  
 165 available satellite at the same resolution (e.g. Landsat-8) or UAVs. Finally, for our crops of interest,  
 166 most images came from the provinces of Quebec (26.46%), Alberta (16.34%), Manitoba (13.80%),  
 167 Saskatchewan (12.39%) and British Columbia (10.92%). This may be due to some crop types being  
 168 more prominent in different climatic zones, such as mixedwood which is highly concentrated in the  
 169 southern regions of Quebec and Ontario, or barley fields being mostly located in the provinces of  
 170 Alberta, Saskatchewan and Manitoba.

171 From the 6,633 geographical points selected, a total of 93,175 images were successfully retrieved,  
 172 which is less than the 132,660 ( $5 \times 6333 \times 4$ ) temporal samples that were theoretically expected over  
 173 the four year period. This was primarily due to the occasional lack of available Sentinel-2 data when  
 174 the image either had too much cloud cover or when the image quality was too low. An example of  
 175 this scenario is depicted in Figure 3. The top row (point 1) shows a location where imagery from all

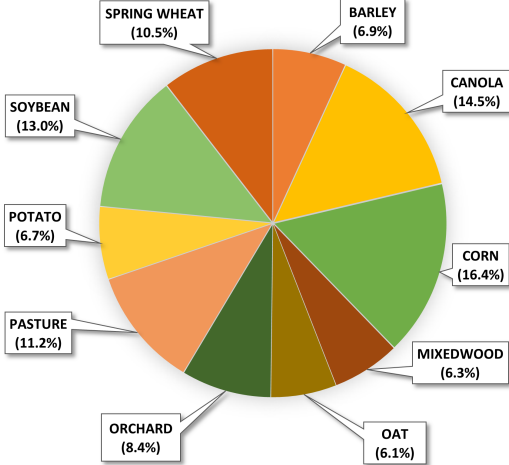


Figure 4: A pie chart showing the distribution of 10 major crop categories from the collected images for 2017 to 2020. Since different crop rotations happened during this period, multiple classes and crop patterns can be observed at a single location over time.

176 5 time steps was available. The middle (point 2) and bottom (point 3) rows illustrate both the cases of  
 177 either missing or low-quality data.

## 178 5 Benchmarking experiments

179 In this section, we present two classification experiments performed using the 2019 version of the  
 180 dataset. In the first experiment, we treated each individual image as a training instance (static image  
 181 classification), similar to the work that was performed in [14]. In the second experiment, we explored  
 182 the use of a temporal image series as an input. Materials, methods and final results are described  
 183 in the sections below. The models were trained either on a Dual Intel Xeon Gold 5120 workstation  
 184 with 64 Gb of RAM and a Titan RTX graphics card (24 Gb of RAM) or Quadro RTX 8000 (48 Gb  
 185 or RAM). Different deep learning models developed in the Python (version 3.8.8) programming  
 186 language were trained using the Keras (version 2.4.3) and TensorFlow (version >=2.1.0) frameworks.  
 187 Each model was trained three times ( $N=3$ ) with a different random seed. We report the average of  
 188 these 3 test results using performance metrics defined in Appendix A.5.

### 189 5.1 Static image classification

190 **ResNet-50, DenseNet, EfficientNet** Different ResNet-50 [13] architectures were employed to  
 191 perform land cover classification. We first used a ResNet-50 pre-trained with ImageNet to reduce  
 192 overfitting of the network. In this case, the base ResNet-50 architecture was supplemented with  
 193 a dense layer (1024 neurons, ReLu activation) followed by a dropout layer (25%), as well as a  
 194 final prediction layer (10 neurons, softmax activation). This network was trained according to the  
 195 following specifications: 30 epochs (10 with the base layers untrainable), a batch-size of 128, an  
 196 rmsprop optimizer and a learning rate set at 0.001. We also trained some ResNet backbones from  
 197 scratch by first using the keras-tuner (version 1.0.1) [30] HyperResNet model to estimate the best  
 198 hyperparameters using the RGB images, including the number of 3- and 4- convolutional blocks,  
 199 the type of pooling layers (maximum or average), the optimizer and the learning rate for 10 epochs  
 200 using RandomSearch. Finally, the best parameters for the untrained ResNet were a total depth of  
 201 4 for the 3-Conv layers and 23 for the 4-Conv layers, an svg optimizer, an average pooling and a  
 202 learning rate of 0.01 which was used for those experiments. More recent network architectures such  
 203 as DenseNet-121 [15] and EfficientNet-B0 [36] were also evaluated. In both cases, we used the  
 204 Keras implementations pre-trained with ImageNet, selecting the more light-weighted architecture to  
 205 avoid over-fitting with our small sized images. In order to be comparable to the ResNet architectures,

206 we added the same top prediction layers (dense layer of 1024 neurons with ReLu, 25% dropout  
 207 and softmax activation) with the exception that a BatchNormalization layer was added after the  
 208 GlobalAveragePooling2D layers of the EfficienNet-B0. Training was performed using the same  
 209 specifications as the ResNets, but with only the top 20 layers of the EfficienNet being trainable (with  
 210 the exception of the BatchNormalization layers set as untrainable). In total, the dataset used for  
 211 training, validation and testing of the static image classification represented 22,413 distinct images  
 212 (Table 1).

## 213 5.2 Dynamic image classification

214 **LRCN and 3D-CNN trained from scratch** For the temporal analysis, we implemented a *Long-*  
 215 *Term Recurrent Convolutional Network* (LRCN) model described by [8] and a 3D-CNN inspired by  
 216 [45] using the Keras deep learning framework. The LRCN network has a CNN as a hierarchical and  
 217 spatial feature extractor coupled with a Long Short-Term Memory (LSTM) model to recognize the  
 218 sequential patterns in the spatio-temporal data. The CNN network was built with 2 ConvLSTM [33]  
 219 (kernel size = (7,7) in layer 1, and (3,3) in layer 2) and Max Pooling blocks, with each one followed  
 220 by a Dropout layer (50% block 1, 50% block 2) and ReLu activation. We determined the number of  
 221 layers for the CNN portion of the network empirically. The output was then reshaped before being  
 222 passed to an LSTM layer, a Dropout layer (50%) and a final prediction layer (10 neurons, softmax  
 223 activation). We tested different combinations of hidden units in the last LSTM layer, which were  
 224 identified as one of the most influential model hyperparameters in [8] (see Table 4 in the Appendix  
 225 A.6). The best overall combination was to use 64 hidden units. Finally, this network architecture was  
 226 trained according to the following specifications: 30 epochs, a batch-size of 32, an rmsprop optimizer  
 227 and a learning rate set at 0.001. For the 3D-CNN, the network was built using a series of 3 Conv3D  
 228 layers with 32 filters, each with kernel size of (1,2,2) followed by BatchNormalization. We dropped  
 229 the MaxPooling3D layers of the original implementation [45] since our temporal series was limited  
 230 in length. These blocks were followed by a GlobalAverage3D pooling layer, a dense layer with 512  
 231 neurons with ReLu activation, a 50% dropout layer and a final prediction layer (10 neurons, softmax  
 232 activation). The training parameters for the 3D-CNN resembled those of other models except for the  
 233 number of epochs which was reduced to 15. For the dynamic experiments, training instances were  
 234 sequences or "image sets" of 3 consecutive images from 2019 from the same data point. In contrast  
 235 to the static experiment, the dataset used for training, validation and testing represented only 7,502  
 236 distinct instances since some locations did not present sequences of 3 consecutive valid images (Table  
 237 1).

Table 1: Number of training, validation and tests samples per experiment (RGB 2019 dataset)

	Experiment type	
	Static image classification	Dynamic image classification
Training	15,612	5,210
Validation	3,349	1,100
Testing	3,452	1,192
Total	22,413	7,502

## 238 5.3 Benchmarking

239 **Results** A summary of our results are presented in Figure 5 and complete results are reported in  
 240 Table 5 of Appendix A.7. For the first static experiment, where we use the pre-trained ResNet-50, the  
 241 training conditions were similar to those in Helber *et al.* [14]. Here, we found that the highest accuracy  
 242 was obtained with the RGB images (0.67) followed by OSAVI (0.62), NDVI45 (0.55), GNDVI (0.52),  
 243 NDVI (0.52) and PSRI (0.48). Other models behaved similarly *i.e.* models trained on RGB images  
 244 performed better than those trained on a single vegetation index which was also observed in another  
 245 study [14]. Those results are, however, lower than some of the accuracies reported by other authors  
 246 for datasets created with Sentinel-2 imagery [6, 43] with higher than 85% accuracy, and higher than

247 98% for land cover classification [14]. Although it was the most modern network, the DenseNet [15]  
248 resulted in the lowest classification accuracy (0.40), while the EfficientNet-B0 [36], with only 5.38  
249 Millions parameters (vs 25.7 Millions for ResNet-50 and 8.1 Millions for DenseNet-121) resulted  
250 in a classification accuracy of 0.53 for RGB images. Training the models for a higher number of  
251 epochs did not improve results. Overall, discrepancies between the classification accuracies were  
252 expected since, by design, some of the crops are not as predominant in the 2019 dataset (e.g. oats,  
253 Figure 4). Moreover, the agricultural landscape of Canada displays variable topologies, field shapes  
254 and sizes which are reflected by discrepancies in management practices (e.g. center pivot irrigation in  
255 the Canadian prairies) [2].

256 In the second experiment, we investigated the possibility of improving agricultural land use  
257 classification using a temporal series of 3 consequent images. The LRCN trained with most vegetation  
258 indices (GNDVI, NDVI, NDVI45 and OSAVI) showed low average precision, ranging from 0.03 to  
259 0.14, and low accuracy from 0.27 to 0.30 (see Table A.7 in the Appendix). However, training using  
260 the PSRI vegetation index resulted in both an average precision (0.45) and accuracy (0.56) higher  
261 than the pre-trained ResNet-50. For the 3D-CNN, the average accuracy were higher when trained  
262 with vegetation indices including PSRI, resulting in values between 0.28 and 0.57, with average  
263 precision still below 0.50. Training the LRCN with RGB images maximized average accuracy (0.77,  
264 Figure 5), representing a 10% higher score than the pre-trained ResNet50 with RGB. Also, the  
265 LRCN classification showed strong average precision (0.61), recall (0.64) and F1-score (0.62). The  
266 3D-CNN, with only 31,082 trainable parameters (vs 14.6 Millions for the LRCN), resulted in an  
267 unexpected higher average accuracy of 0.77, with similar average precision (0.61), recall (0.62) and  
268 F1-score (0.60). Those results are similar to the 77% accuracy obtained by Amani *et al.* [2] using  
269 Sentinel-1, -2 images, and an ANN on the GEE platform. In their case, they used NDVI and the  
270 Normalized Difference Water Index (NDWI) as their features derived from Sentinel-2 data. They  
271 also used 197,634 images to represent their 17 crop classes (including corn, soybean and potato).  
272 Different reasons can explain the poor performance obtained by our models trained with a singular  
273 vegetation index. For NDVI and related indices [7, 11], a saturation of the index occurs for different  
274 cultures when they attain maturity (end of vegetative stage). In contrast, the PSRI index measures  
275 the senescence or ripening of the crop cover, and thus, might present more learnable features in the  
276 months of July, August and September, more present in our dataset [27].

277 When comparing both of the dynamic classification models, the 3D-CNN, although having a simplistic  
278 and un-optimized architecture in our implementation, showed similar results to the more complex  
279 LRCN architecture composed of ConvLSTM layers. Similar results were obtained in [29] when  
280 analyzing temporal cardiac magnetic resonance images, with results favoring either model depending  
281 on the prior data augmentation techniques. Thus, more research is required to improve these network  
282 architectures and optimize them for use with this new dataset. Nevertheless, the difference in the  
283 number of parameters is  $\sim 450 \times$  more for the LRCN network compared to the 3D-CNN, which  
284 leads us to prefer the latter architecture since the gains in accuracy are limited when comparing model  
285 size. However, the similar results obtained by the two network architectures might also be due to  
286 some limitations in the number of training samples which could be solved though data augmentation  
287 as demonstrated in [29]. One limitation arising from the current benchmark is that we did not evaluate  
288 classification of the same location (i.e static vs dynamic) since misclassification could happen in one  
289 static image through the season, thus needing a rule-based or ensemble algorithm to correctly identify  
290 the resulting class in order to compare a period of 3 months.

## 291 6 Contributions and Future Work

292 The availability of annotated multitemporal images which can accurately represent, according to [9],  
293 *i*) all multitemporal classes, *ii*) the inter-relation between classes along the time-series with a reliable  
294 statistic, and *iii*) the high temporal and spatial variability in large scenes is scarce. The *Canadian*  
295 *Cropland Dataset* bridges this gap by directly addressing points *i*) and *iii*) in an agricultural context.  
296 One potential negative societal impact could be the development of models allowing the advance  
297 monitoring of crop conditions and agricultural fraud detection. However, one positive impact could be

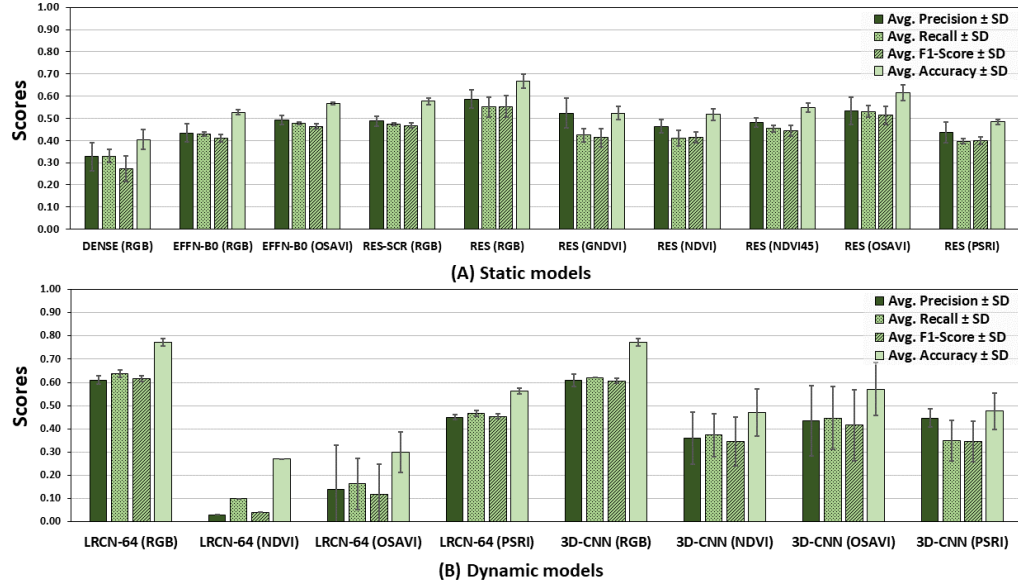


Figure 5: Summary of classification results for models trained on the 2019 subsets. In A, results for the static image classification and in B, results for the dynamic image classification. Full results are presented in Table 5 in the Appendix. Abbreviations: DENSE (DenseNet-121 pre-trained with ImageNet), EFFN-B0 (EfficientNet-B0 pre-trained with ImageNet), RES (ResNet-50 pre-trained with ImageNet), RES-SCR (ResNet-50 trained from scratch). Results reported are average  $\pm$  standard deviation (SD) of triplicate experiments with different starting random seeds.

298 the classification of land use based on different crop rotations. Crop rotation is becoming central to the  
 299 study of higher land resilience, carbon sequestration and biodiversity [23]. Thus, this dataset might  
 300 be used to develop new models fostering large-scale studies of biological conservation measures.  
 301 Furthermore, different opportunities exist to augment the current dataset using the provided scripts.  
 302 First, the USDA CropScape - Cropland Data Layer [4] is also available on GEE. Incorporating more  
 303 field samples from the data layer could allow a greater representation of both the diversity of North  
 304 American croplands and their topology. Second, a European cropland layer known as the *Denmark*  
 305 *LPIS dataset* was used by [18] to compare the loss of agricultural land, and could also be used to  
 306 increase the dataset scope beyond North America. Finally, ancillary data such as meteorological  
 307 data could be added using the location information. This additional information could help to better  
 308 understand vegetation phenology correlated with the included vegetation indices layers.

## 309 7 Conclusion

310 The release of Google Earth Engine and Sentinel-2 imagery to the RS research community have  
 311 catalyzed the creation of new tools, models and data sources for land cover and land use classification.  
 312 We exploited these tools by creating a multitemporal patch-based dataset of Canadian cropland  
 313 images and identified the challenges that arise when curating a large dataset using unprocessed  
 314 satellite imagery. Furthermore, we performed benchmarking tests on a subset of the dataset using two  
 315 different strategies: static (e.g. ResNet, DenseNet, EfficientNet) or dynamic series of images (e.g.  
 316 3D-CNN, LRCN). These tests demonstrated that incorporating spatio-temporal sequences resulted in  
 317 better land cover classification accuracy using our dataset, while reducing the number of required  
 318 training instances and training parameters. We believe that this novel dataset can be used in the  
 319 creation of robust environmental models that can help to better understand and map complex and  
 320 dynamic agricultural regions.

321 **Acknowledgments** This work was supported by Agriculture and Agri-Food Canada. All authors  
322 contributed equally to the production of this manuscript.

323 **References**

- 324 [1] Agriculture and Agri-Food Canada. Annual crop inventory. [https://open.canada.ca/en/](https://open.canada.ca/en/apps/aafc-crop-inventory)  
325 apps/aafc-crop-inventory, 2016.
- 326 [2] Meisam Amani, Mohammad Kakooei, Armin Moghimi, Arsalan Ghorbanian, Babak Ranjgar,  
327 Sahel Mahdavi, Andrew Davidson, Thierry Fisette, Patrick Rollin, Brian Brisco, and Ali  
328 Mohammadzadeh. Application of google earth engine cloud computing platform, sentinel  
329 imagery, and neural networks for crop mapping in canada. *Remote Sensing*, 12:3561, 11 2020.
- 330 [3] J.A. Benediktsson, M. Pesaresi, and K. Amason. Classification and feature extraction for remote  
331 sensing images from urban areas based on morphological transformations. *IEEE Transactions*  
332 on Geoscience and Remote Sensing, 41(9):1940–1949, Sep. 2003.
- 333 [4] Claire Boryan, Zhengwei Yang, Rick Mueller, and Mike Craig. Monitoring us agriculture: the  
334 us department of agriculture, national agricultural statistics service, cropland data layer program.  
335 *Geocarto International*, 26(5):341–358, 2011.
- 336 [5] Francesca Bovolo and Lorenzo Bruzzone. The time variable in data fusion: A change detection  
337 perspective. *IEEE Geoscience and Remote Sensing Magazine*, 3:8–26, 9 2015.
- 338 [6] Manuel Campos-Taberner, Francisco Javier García-Haro, Beatriz Martínez, Emma Izquierdo-  
339 Verdiguier, Clement Atzberger, Gustau Camps-Valls, and María Amparo Gilabert.  
340 Understanding deep learning in land use classification based on sentinel-2 time series. *Scientific*  
341 *reports*, 10(1):1–12, 2020.
- 342 [7] Jesús Delegido, Jochem Verrelst, Luis Alonso, and José Moreno. Evaluation of sentinel-  
343 2 red-edge bands for empirical estimation of green LAI and chlorophyll content. *Sensors*,  
344 11:7063–7081, 7 2011.
- 345 [8] Jeff Donahue, Lisa Anne Hendricks, Marcus Rohrbach, Subhashini Venugopalan, Sergio  
346 Guadarrama, Kate Saenko, and Trevor Darrell. Long-term recurrent convolutional networks  
347 for visual recognition and description. *IEEE Transactions on Pattern Analysis and Machine*  
348 *Intelligence*, 39:677–691, 11 2017.
- 349 [9] Pedram Ghamisi, Behnoor Rasti, Naoto Yokoya, Qunming Wang, Bernhard Hofle, Lorenzo  
350 Bruzzone, Francesca Bovolo, Mingmin Chi, Katharina Anders, Richard Gloaguen, Peter M.  
351 Atkinson, and Jon Atli Benediktsson. Multisource and multitemporal data fusion in remote  
352 sensing: A comprehensive review of the state of the art. *IEEE Geoscience and Remote Sensing*  
353 *Magazine*, 7:6–39, 3 2019.
- 354 [10] Rahul Ghosh, Praveen Ravirathinam, Xiaowei Jia, Ankush Khandelwal, David J. Mulla, and  
355 Vipin Kumar. Calcrop21: A georeferenced multi-spectral dataset of satellite imagery and crop  
356 labels. *2021 IEEE International Conference on Big Data (Big Data)*, pages 1625–1632, 2021.
- 357 [11] Anatoly A. Gitelson, Yoram J. Kaufman, and Mark N. Merzlyak. Use of a green channel  
358 in remote sensing of global vegetation from eos-modis. *Remote Sensing of Environment*,  
359 58(3):289–298, 1996.
- 360 [12] N. Gorelick, M. Hancher, M. Dixon, S. Ilyushchenko, D. Thau, and R. Moore. Google earth  
361 engine: Planetary-scale geospatial analysis for everyone. *Remote Sensing of Environment*, 2017.
- 362 [13] Kaiming He, Xiangyu Zhang, Shaoqing Ren, and Jian Sun. Deep residual learning for image  
363 recognition. In *IEEE Conference on Computer Vision and Pattern Recognition*, pages 770–778,  
364 12 2016.

- 365 [14] Patrick Helber, Benjamin Bischke, Andreas Dengel, and Damian Borth. Eurosat: A novel  
 366 dataset and deep learning benchmark for land use and land cover classification. *IEEE Journal*  
 367 *of Selected Topics in Applied Earth Observations and Remote Sensing*, 12:2217–2226, 7 2019.
- 368 [15] Gao Huang, Zhuang Liu, and Kilian Q. Weinberger. Densely connected convolutional networks.  
 369 *CoRR*, abs/1608.06993, 2016.
- 370 [16] Xiuping Jia, Bor-Chen Kuo, and Melba M. Crawford. Feature mining for hyperspectral image  
 371 classification. *Proceedings of the IEEE*, 101(3):676–697, March 2013.
- 372 [17] Jinha Jung, Murilo Maeda, Anjin Chang, Mahendra Bhandari, Akash Ashapure, and Juan  
 373 Landivar-Bowles. The potential of remote sensing and artificial intelligence as tools to improve  
 374 the resilience of agriculture production systems. *Current Opinion in Biotechnology*, 70:15–22,  
 375 8 2021.
- 376 [18] Eva Kerselaers and Gregor Levin. Applying lpis data to assess loss of agricultural land –  
 377 experiences from flanders and denmark. *Geografisk Tidsskrift-Danish Journal of Geography*,  
 378 119(1):17–29, 2019.
- 379 [19] Reza Khatami, Giorgos Mountakis, and Stephen V. Stehman. A meta-analysis of remote  
 380 sensing research on supervised pixel-based land-cover image classification processes: General  
 381 guidelines for practitioners and future research. *Remote Sensing of Environment*, 177:89–100, 5  
 382 2016.
- 383 [20] Lukas Kondmann, Aysim Toker, Marc Rußwurm, Andrés Camero, Devis Peressuti, Grega  
 384 Milcinski, Pierre-Philippe Mathieu, Nicolas Longépé, Timothy Davis, Giovanni Marchisio,  
 385 Laura Leal-Taixé, and Xiao Xiang Zhu. DENETHOR: The dynamicearthNET dataset for  
 386 harmonized, inter-operable, analysis-ready, daily crop monitoring from space. In *Thirty-fifth*  
 387 *Conference on Neural Information Processing Systems Datasets and Benchmarks Track (Round*  
 388 *2)*, 2021.
- 389 [21] Lalit Kumar and Onisimo Mutanga. Google earth engine applications since inception: Usage,  
 390 trends, and potential. *Remote Sensing*, 10:1509, 10 2018.
- 391 [22] Natalia Kussul, Mykola Lavreniuk, Sergii Skakun, and Andrii Shelestov. Deep learning  
 392 classification of land cover and crop types using remote sensing data. *IEEE Geoscience and*  
 393 *Remote Sensing Letters*, 14:778–782, 5 2017.
- 394 [23] Minghui Li, Junjie Guo, Tao Ren, Gongwen Luo, Qirong Shen, Jianwei Lu, Shiwei Guo, and  
 395 Ning Ling. Crop rotation history constrains soil biodiversity and multifunctionality relationships.  
 396 *Agriculture, Ecosystems & Environment*, 319:107550, 2021.
- 397 [24] Ruirui Li, Wenjie Liu, Lei Yang, Shihao Sun, Wei Hu, Fan Zhang, and Wei Li. DeepUNet:  
 398 A deep fully convolutional network for pixel-level sea-land segmentation. *IEEE Journal of*  
 399 *Selected Topics in Applied Earth Observations and Remote Sensing*, 11:3954–3962, 11 2018.
- 400 [25] Khairiya Mudrik Masoud, Claudio Persello, and Valentyn A. Tolpekin. Delineation of  
 401 agricultural field boundaries from sentinel-2 images using a novel super-resolution contour  
 402 detector based on fully convolutional networks. *Remote Sensing*, 12:59, 1 2020.
- 403 [26] Vittorio Mazzia, Aleem Khaliq, and Marcello Chiaberge. Improvement in land cover and  
 404 crop classification based on temporal features learning from sentinel-2 data using recurrent-  
 405 convolutional neural network (R-CNN). *Applied Sciences*, 10:238, 1 2020.
- 406 [27] Mark N Merzlyak, Anatoly A Gitelson, Olga B Chivkunova, and Victor Yu Rakitin. Non-  
 407 destructive optical detection of pigment changes during leaf senescence and fruit ripening.  
 408 *Physiologia Plantarum*, 106:135–141, 1999.

- 409 [28] Natural Resources Canada. Land cover and land use. <https://www.nrcan.gc.ca/maps-tools-and-publications/satellite-imagery-and-air-photos/remote-sensing-tutorials/land-cover-land-use/>, 2015.
- 410
- 411
- 412 [29] Ilkay Oksuz, Bram Ruijsink, Esther Puyol-Antón, James R. Clough, Gastao Cruz, Aurelien Bustin, Claudia Prieto, Rene Botnar, Daniel Rueckert, Julia A. Schnabel, and Andrew P. King. Automatic cnn-based detection of cardiac mr motion artefacts using k-space data augmentation and curriculum learning. *Medical Image Analysis*, 55:136–147, 2019.
- 413
- 414
- 415
- 416 [30] Tom O’Malley, Elie Bursztein, James Long, François Chollet, Haifeng Jin, Luca Invernizzi, et al. Keras Tuner. <https://github.com/keras-team/keras-tuner>, 2019.
- 417
- 418 [31] Geneviève Rondeaux, Michael Steven, and Frédéric Baret. Optimization of soil-adjusted vegetation indices. *Remote Sensing of Environment*, 55(2):95–107, 1996.
- 419
- 420 [32] Jr. Rouse, J. W., R. H. Haas, J. A. Schell, and D. W. Deering. *Monitoring Vegetation Systems in the Great Plains with Erts*, volume 351, page 309. NASA Special Publication, 1974.
- 421
- 422 [33] Xingjian Shi, Zhourong Chen, Hao Wang, Dit-Yan Yeung, Wai-kin Wong, and Wang-chun Woo. Convolutional lstm network: A machine learning approach for precipitation nowcasting. In *Proceedings of the 28th International Conference on Neural Information Processing Systems - Volume 1*, NIPS’15, page 802–810, Cambridge, MA, USA, 2015. MIT Press.
- 423
- 424
- 425
- 426 [34] Hunsoo Song, Yonghyun Kim, and Yongil Kim. A patch-based light convolutional neural network for land-cover mapping using landsat-8 images. *Remote Sensing*, 11:114, 1 2019.
- 427
- 428 [35] Gencer Sumbul, Arne de Wall, Tristan Kreuziger, Filipe Marcelino, Hugo Costa, Pedro Benevides, Mario Caetano, Begüm Demir, and Volker Markl. Bigearthnet-mm: A large scale multi-modal multi-label benchmark archive for remote sensing image classification and retrieval. *CoRR*, abs/2105.07921, 2021.
- 429
- 430
- 431
- 432 [36] Mingxing Tan and Quoc V. Le. Efficientnet: Rethinking model scaling for convolutional neural networks. *CoRR*, abs/1905.11946, 2019.
- 433
- 434 [37] The European Space Agency. Radiometric resolutions. <https://sentinel.esa.int/web/sentinel/user-guides/sentinel-2-msi/resolutions/radiometric>, 2021.
- 435
- 436 [38] Gabriel Tseng, Ivan Zvonkov, Catherine Lilian Nakalembe, and Hannah Kerner. Cropharvest: A global dataset for crop-type classification. In *Thirty-fifth Conference on Neural Information Processing Systems Datasets and Benchmarks Track (Round 2)*, 2021.
- 437
- 438
- 439 [39] Qunming Wang and Peter M. Atkinson. Spatio-temporal fusion for daily sentinel-2 images. *Remote Sensing of Environment*, 204:31–42, 2018.
- 440
- 441 [40] Mathias Wessel, Melanie Brandmeier, and Dirk Tiede. Evaluation of different machine learning algorithms for scalable classification of tree types and tree species based on sentinel-2 data. *Remote Sensing*, 10:1419, 9 2018.
- 442
- 443
- 444 [41] Jinru Xue and Baofeng Su. Significant remote sensing vegetation indices: A review of developments and applications. *Journal of Sensors*, 2017, 2017.
- 445
- 446 [42] Liangpei Zhang, Lefei Zhang, and Bo Du. Deep learning for remote sensing data: A technical tutorial on the state of the art. *IEEE Geoscience and Remote Sensing Magazine*, 4:22–40, 6 2016.
- 447
- 448
- 449 [43] Hongwei Zhao, Sibo Duan, Jia Liu, Liang Sun, and Louis Reymondin. Evaluation of five deep learning models for crop type mapping using sentinel-2 time series images with missing information. *Remote Sensing*, 13(14):2790, 2021.
- 450
- 451

- 452 [44] Xiao Xiang Zhu, Devis Tuia, Lichao Mou, Gui Song Xia, Liangpei Zhang, Feng Xu, and  
453 Friedrich Fraundorfer. Deep learning in remote sensing: A comprehensive review and list of  
454 resources. *IEEE Geoscience and Remote Sensing Magazine*, 5:8–36, 12 2017.
- 455 [45] Hasib Zunair, Aimon Rahman, Nabeel Mohammed, and Joseph Paul Cohen. Uniformizing  
456 techniques to process ct scans with 3d cnns for tuberculosis prediction. In Islem Rekik, Ehsan  
457 Adeli, Sang Hyun Park, and Maria del C. Valdés Hernández, editors, *Predictive Intelligence in*  
458 *Medicine*, pages 156–168, Cham, 2020. Springer International Publishing.

459    **Checklist**

- 460    1. For all authors...
  - 461    (a) Do the main claims made in the abstract and introduction accurately reflect the paper's contributions and scope? **[Yes]**
  - 462    (b) Did you describe the limitations of your work? **[Yes]** Missing data and unbalanced classes - see Results section
  - 463    (c) Did you discuss any potential negative societal impacts of your work? **[Yes]** See section - Uses and Future Work
  - 464    (d) Have you read the ethics review guidelines and ensured that your paper conforms to them? **[Yes]**
- 465    2. If you are including theoretical results...
  - 466    (a) Did you state the full set of assumptions of all theoretical results? **[N/A]**
  - 467    (b) Did you include complete proofs of all theoretical results? **[N/A]**
- 468    3. If you ran experiments (e.g. for benchmarks)...
  - 469    (a) Did you include the code, data, and instructions needed to reproduce the main experimental results (either in the supplemental material or as a URL)? **[Yes]** See the included github:<https://github.com/bioinfoUQAM/Canadian-cropland-dataset>
  - 470    (b) Did you specify all the training details (e.g., data splits, hyperparameters, how they were chosen)? **[Yes]** See section: Benchmarking experiments
  - 471    (c) Did you report error bars (e.g., with respect to the random seed after running experiments multiple times)? **[Yes]** Yes, all experiments were done at least in triplicates - Section Benchmarking experiments
  - 472    (d) Did you include the total amount of compute and the type of resources used (e.g., type of GPUs, internal cluster, or cloud provider)? **[Yes]** Yes, head of section Benchmarking experiments
- 473    4. If you are using existing assets (e.g., code, data, models) or curating/releasing new assets...
  - 474    (a) If your work uses existing assets, did you cite the creators? **[Yes]** e.g. keras-tuner, ResNet, EfficientNet, etc.
  - 475    (b) Did you mention the license of the assets? **[Yes]** Through citation in the manuscript and the datasheet in the Appendix.
  - 476    (c) Did you include any new assets either in the supplemental material or as a URL? **[Yes]** Some common python library e.g. Pandas, Numpy and other are only listed on the Github page
  - 477    (d) Did you discuss whether and how consent was obtained from people whose data you're using/curating? **[N/A]** The scripts and content was developed by us. The data and labels both come from open sourced databases (GEE and the Canadian ACI).
  - 478    (e) Did you discuss whether the data you are using/curating contains personally identifiable information or offensive content? **[Yes]** The content do not contains all of the above.
- 479    5. If you used crowdsourcing or conducted research with human subjects...
  - 480    (a) Did you include the full text of instructions given to participants and screenshots, if applicable? **[N/A]**
  - 481    (b) Did you describe any potential participant risks, with links to Institutional Review Board (IRB) approvals, if applicable? **[N/A]**
  - 482    (c) Did you include the estimated hourly wage paid to participants and the total amount spent on participant compensation? **[N/A]**

504 **A Appendix**

505 **A.1 Sentinel-2 reflectance bands**

Table 2: List of the main spectral bands captured by Sentinel-2 and their respective wavelengths.

Band name	Spatial resolution (pixel/m)	Central wavelength (nm)	Description
B1	60	444	Aerosols
B2	10	497	Blue
B3	10	560	Green
B4	10	665	Red
B5	20	704	Red Edge 1
B6	20	740	Red Edge 2
B7	20	783	Red Edge 3
B8	10	835	NIR
B8A	20	865	Red Edge 4
B9	60	945	Water vapor
B11	20	1614	SWIR1
B12	20	2202	SWIR2

506 **A.2 Canadian Annual Crop Inventory accuracy table**

Table 3: Summary of the ACI crop class accuracy for each year and province.

Province	2016	2017	2018	2019	2020	Average (2016-2020)
Alberta	90.83	94.15	91.95	91.29	88.94	91.43
British Columbia	82.27	92.79	93.09	89.35	85.16	88.53
Manitoba	92.44	93.10	94.61	94.27	93.47	93.58
New Brunswick	89.66	84.29	88.83	91.90	95.74	90.08
Newfoundland	94.51	91.83	93.84	91.00	95.08	93.25
Nova Scotia	90.59	89.49	92.50	89.10	NaN	90.42
Ontario	88.98	85.36	91.99	85.64	88.26	88.05
Prince Edward Island	82.44	91.61	81.92	89.78	85.85	86.32
Quebec	91.17	90.26	92.28	91.80	91.2	91.34
Saskatchewan	92.26	93.71	91.65	91.63	93.87	92.62
Average (all provinces)	89.52	90.66	91.27	90.58	90.8	<b>90.56</b>

Source: Annual Crop Inventory - Data Product Specification - As of June 7th, 2022. Missing values are imputed using the mean of each row. [1]

507 **A.3 Definition of vegetation indices**

508 **NDVI** The *Normalized Difference Vegetation Index* (NDVI) is one of the most predominantly used  
509 indicators of plant growth and health. It correlates with the amount of chlorophyll emitted by a plant  
510 [32]. NDVI is defined as:

$$NDVI = \frac{\rho_{NIR} - \rho_{red}}{\rho_{NIR} + \rho_{red}} \quad (1)$$

511 Where  $\rho_{NIR}$  is equal to the NIR band and  $\rho_{red}$  is the visible red band (represented by bands B8 and  
512 B4 in Table 2, respectively).

513 **NDVI45** The *NDVI45* vegetation index is a revised version of the NDVI developed by [7]. It is  
514 strongly correlated with the leaf area index (LAI), which is an estimate of the amount of biomass and  
515 vegetative evapotranspiration, and provides information regarding the structure of a canopy. NDVI45  
516 is defined as:

$$NDVI45 = \frac{R_{704} - \rho_{red}}{R_{704} + \rho_{red}} \quad (2)$$

517 Where  $R_{704}$  is the NIR spectral band centered at 704 nm (B5).

518 **GNDVI** The *Green Normalized Difference Vegetation Index* (GNDVI) was shown to correlate to  
 519 the rate of photosynthesis and is used to monitor plant stress [11]. GNDVI is calculated in a way that  
 520 is analogous to NDVI, however the red band is replaced by the green band ( $\rho_{green}$ ):

$$GNDVI = \frac{\rho_{NIR} - \rho_{green}}{\rho_{NIR} + \rho_{green}} \quad (3)$$

521 **PSRI** The *Plant Senescence Reflectance Index* (PSRI) is used to measure the onset, the stage,  
 522 and the relative rates of the senescence or ripening of a crop cover. An increase in PSRI indicates  
 523 heightened canopy stress [27]. PSRI is defined by the equation:

$$PSRI = \frac{\rho_{red} - \rho_{blue}}{R_{750}} \quad (4)$$

524 Where  $R_{750}$  is the NIR spectral band centered at 750 nm (B6).

525 **OSAVI** In conditions when vegetation is low and soil properties are unknown, indices like the  
 526 NDVI can be subject to bias due to high levels of reflection. The *Optimized Soil-Adjusted Variation*  
 527 *Index* (OSAVI) was created to provide an estimate of biomass that is more resilient when faced with  
 528 soil and atmospheric effects [31].

$$OSAVI = \frac{\rho_{NIR} - \rho_{red}}{\rho_{NIR} + \rho_{red} + 0.16} \quad (5)$$

529 **A.4 An example image from the *Canadian Cropland Dataset*.**

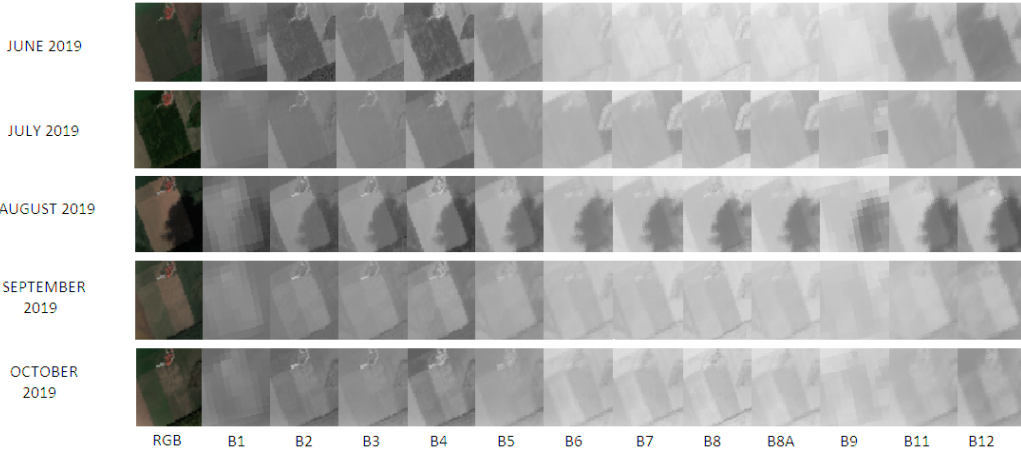


Figure 6: Example of a Sentinel-2 image for a barley field in Ontario, Canada. The different bands (B1 to B12) represent the median of the pixels for each month.

530 **A.5 Definition of performance metrics**

531 **Accuracy** To evaluate the performance of each classification algorithm, a selection of performance  
 532 metrics were used. *Accuracy* (equation 6) is an important metric that represents the capacity of an

533 algorithm to correctly classify instances. Although it is a powerful indicator of overall performance,  
 534 accuracy alone is not enough to determine the strength of an algorithm and whether it has correctly  
 535 learned the task at hand. Accuracy is defined as:

$$Accuracy = \frac{\Sigma TP + \Sigma TN}{\Sigma TP + \Sigma TN + \Sigma FP + \Sigma FN}, \quad (6)$$

536 where  $TP$  and  $TN$  are the number of true positive and true negative classifications, respectively;  
 537 and  $FP$  and  $FN$  are the number of false positive and false negative classifications, respectively.  
 538 Accuracy, like all metrics, is often multiplied by 100 to yield a percentage.

539 **Precision** *Precision* (equation 7), also referred to as positive predictive value (PPV), is used to  
 540 determine the capacity of an algorithm to correctly identify positive cases with respect to all the cases  
 541 the algorithm has classified as positive. It is calculated by dividing the number of true positives by  
 542 the number of predicted positives, which itself is a sum of  $TP$  and  $FP$ . Precision is defined as:

$$Precision = \frac{\Sigma TP}{\Sigma TP + \Sigma FP}. \quad (7)$$

543 Precision is an indicator of how reproducible and repeatable a measurement is under unchanged  
 544 conditions and is used to evaluate the exactness of a model.

545 **Recall** *Recall* (equation 8) is the fraction of relevant instances that have been correctly identified  
 546 ( $TP$ ) over the total amount of relevant instances ( $TP$  and  $FN$ ). Recall and precision are typically used  
 547 in unison to report the performance of a classification system. Precision indicates the quality of the  
 548 positive prediction capability of the model, while recall indicates the completeness or quantity of  
 549 correct predictions with respect to all positive instances present. High precision would mean that the  
 550 algorithm returned a greater amount of relevant results than irrelevant ones, while a high recall value  
 551 would mean that the algorithm returned most of the relevant results.

$$Recall = \frac{\Sigma TP}{\Sigma TP + \Sigma FN} \quad (8)$$

552 **F1-Score** *F1-Score* or *F-measure* (equation 9) is a metric that combines both precision and recall  
 553 into a single encompassing metric. This weighted average is bounded between 0 - representing the  
 554 worst classification and 1 - representing the best.

$$F1 - Score = 2 \times \frac{Precision \times Recall}{Precision + Recall} \quad (9)$$

555 **A.6 LRCN performance metrics (RGB 2019 dataset)**

Table 4: LRCN performance metrics (RGB 2019 dataset)

Metrics	Number of hidden LSTM units in the last layer.			
	32	64	128	256
Avg. Precision	0.59	0.61	0.59	0.62
Avg. Recall	0.62	0.64	0.62	0.62
Avg. F1-Score	0.60	0.62	0.60	0.61
Avg. Accuracy	0.76	0.77	0.74	0.74

556 A.7 Complete summary of performance metrics for all models

Table 5: Model performance metrics (RGB 2019 dataset)\*

Models/Metrics	Precision	Recall	F1-Score	Accuracy
<i>Dynamic</i>				
<b>LRCN-64 (RGB)</b>	$0.610 \pm 0.017$	$0.637 \pm 0.015$	$0.617 \pm 0.012$	<b><math>0.774 \pm 0.014</math></b>
<b>LRCN-64 (GNDVI)</b>	$0.030 \pm 0.000$	$0.100 \pm 0.000$	$0.040 \pm 0.000$	$0.277 \pm 0.006$
<b>LRCN-64 (NDVI)</b>	$0.030 \pm 0.000$	$0.100 \pm 0.000$	$0.040 \pm 0.000$	$0.270 \pm 0.000$
<b>LRCN-64 (NDVI45)</b>	$0.123 \pm 0.162$	$0.180 \pm 0.139$	$0.127 \pm 0.150$	$0.313 \pm 0.101$
<b>LRCN-64 (OSAVI)</b>	$0.140 \pm 0.191$	$0.163 \pm 0.110$	$0.117 \pm 0.133$	$0.300 \pm 0.087$
<b>LRCN-64 (PSRI)</b>	$0.450 \pm 0.010$	$0.467 \pm 0.012$	$0.453 \pm 0.012$	$0.563 \pm 0.012$
<b>3D-CNN (RGB)</b>	$0.610 \pm 0.026$	$0.620 \pm 0.000$	$0.607 \pm 0.012$	<b><math>0.773 \pm 0.012</math></b>
<b>3D-CNN (GNDVI)</b>	$0.287 \pm 0.085$	$0.250 \pm 0.066$	$0.200 \pm 0.069$	$0.313 \pm 0.067$
<b>3D-CNN (NDVI)</b>	$0.360 \pm 0.113$	$0.373 \pm 0.093$	$0.347 \pm 0.104$	$0.470 \pm 0.100$
<b>3D-CNN (NDVI45)</b>	$0.467 \pm 0.065$	$0.387 \pm 0.031$	$0.377 \pm 0.040$	$0.530 \pm 0.026$
<b>3D-CNN (OSAVI)</b>	$0.433 \pm 0.151$	$0.447 \pm 0.136$	$0.417 \pm 0.153$	$0.570 \pm 0.114$
<b>3D-CNN (PSRI)</b>	$0.447 \pm 0.040$	$0.350 \pm 0.087$	$0.347 \pm 0.087$	$0.477 \pm 0.078$
<i>Static</i>				
<b>DENSENET-121 (RGB)</b>	$0.327 \pm 0.064$	$0.330 \pm 0.030$	$0.273 \pm 0.058$	<b><math>0.403 \pm 0.045</math></b>
<b>DENSENET-121 (GNDVI)</b>	$0.057 \pm 0.029$	$0.133 \pm 0.042$	$0.060 \pm 0.044$	$0.150 \pm 0.053$
<b>DENSENET-121 (NDVI)</b>	$0.217 \pm 0.067$	$0.183 \pm 0.015$	$0.140 \pm 0.030$	$0.260 \pm 0.026$
<b>DENSENET-121 (NDVI45)</b>	$0.187 \pm 0.055$	$0.257 \pm 0.035$	$0.180 \pm 0.036$	$0.293 \pm 0.032$
<b>DENSENET-121 (OSAVI)</b>	$0.213 \pm 0.021$	$0.210 \pm 0.044$	$0.153 \pm 0.038$	$0.257 \pm 0.051$
<b>DENSENET-121 (PSRI)</b>	$0.160 \pm 0.020$	$0.197 \pm 0.015$	$0.147 \pm 0.012$	$0.260 \pm 0.017$
<b>EFFN-B0 (RGB)</b>	$0.433 \pm 0.042$	$0.430 \pm 0.010$	$0.410 \pm 0.017$	<b><math>0.527 \pm 0.012</math></b>
<b>EFFN-B0 (GNDVI)</b>	$0.427 \pm 0.015$	$0.430 \pm 0.010$	$0.413 \pm 0.015$	$0.527 \pm 0.006$
<b>EFFN-B0 (NDVI)</b>	$0.343 \pm 0.055$	$0.310 \pm 0.052$	$0.303 \pm 0.046$	$0.400 \pm 0.053$
<b>EFFN-B0 (NDVI45)</b>	$0.470 \pm 0.017$	$0.460 \pm 0.010$	$0.443 \pm 0.012$	$0.543 \pm 0.006$
<b>EFFN-B0 (OSAVI)</b>	$0.493 \pm 0.021$	$0.477 \pm 0.006$	$0.463 \pm 0.012$	$0.567 \pm 0.006$
<b>EFFN-B0 (PSRI)</b>	$0.417 \pm 0.029$	$0.393 \pm 0.006$	$0.380 \pm 0.010$	$0.483 \pm 0.006$
<b>RES-SCR (RGB)</b>	$0.487 \pm 0.021$	$0.473 \pm 0.006$	$0.467 \pm 0.012$	<b><math>0.577 \pm 0.015</math></b>
<b>RES-SCR (PSRI)</b>	$0.333 \pm 0.042$	$0.297 \pm 0.029$	$0.277 \pm 0.029$	$0.393 \pm 0.006$
<b>RES-SCR (NDVI)</b>	$0.280 \pm 0.036$	$0.293 \pm 0.012$	$0.257 \pm 0.021$	$0.370 \pm 0.026$
<b>RES (RGB)</b>	$0.587 \pm 0.040$	$0.550 \pm 0.044$	$0.553 \pm 0.047$	<b><math>0.667 \pm 0.032</math></b>
<b>RES (GNDVI)</b>	$0.523 \pm 0.067$	$0.423 \pm 0.031$	$0.413 \pm 0.040$	$0.523 \pm 0.031$
<b>RES (NDVI)</b>	$0.463 \pm 0.031$	$0.410 \pm 0.036$	$0.413 \pm 0.025$	$0.517 \pm 0.025$
<b>RES (NDVI45)</b>	$0.480 \pm 0.020$	$0.453 \pm 0.015$	$0.443 \pm 0.023$	$0.547 \pm 0.021$
<b>RES (OSAVI)</b>	$0.533 \pm 0.060$	$0.530 \pm 0.026$	$0.513 \pm 0.040$	$0.617 \pm 0.035$
<b>RES (PSRI)</b>	$0.437 \pm 0.046$	$0.397 \pm 0.012$	$0.400 \pm 0.017$	$0.483 \pm 0.012$

\*LRCN-64 (LRCN with 64 hidden units in the last LSTM layer - see Table 4), RES (pre-trained ResNet-50), RES-SCR (ResNet trained from scratch, EFFN-B0 (EfficientNet-B0) - See section *Static and Dynamic image classification*). The presented scores are average  $\pm$  standard deviation (SD) of triplicate experiments with different starting random seeds. Results in **bold** are the average accuracy of the models trained with the RGB 2019 dataset. All models were implemented using Keras and Tensorflow.

557 **A.8 Canadian Cropland Dataset - License**

558 **Montreal Data License (MDL)**

559 The following licensing language is made available under CC-BY4. Attribution should be made to  
560 Montreal Data License (MDL), or License language based on Montreal Data License.

561 The authors are not legal advisors to the individuals and entities making use of these licensing terms.  
562 The licensing terms can be combined as needed to match the rights conferred by the licensor.

563 The language below assumes that all rights are granted, however each right should be conferred or  
564 not based on the users intent.

565 *Data License for use in AI and ML:*

566 This license covers the Data made available by Lessor to you (License) under the following terms.  
567 Licensees use of the data consists acceptance of the terms of this license agreement (License).

568 **1. Definitions**

569 (a) *Data* means the informational content (individually or as a whole) made available by  
570 Lessor.

571 (b) *Model* means machine-learning or artificial-intelligence based algorithms, or assemblies  
572 thereof that, in combination with different techniques, may be used to obtain certain  
573 results. Without limitation, such results can be insights on past data patterns, predictions  
574 on future trends or more abstract results.

575 (c) *Output* means the results of operating a Trained Model as embodied in informational  
576 content resulting therefrom.

577 (d) *Representation* is a transformation of a piece of data into a different form. Good  
578 representations can be used as input to perform useful tasks.

579 (e) *Labelled Data* means the associated metadata and informational content derived from  
580 Data which identify, comment or otherwise derive information from Data, such as tags  
581 and labels.

582 (f) *Lessor* means the individual or entity making the Data available to you.

583 (g) *Third Parties* means individuals or entities that are not under common control with  
584 Licensee.

585 (h) *Train* means to expose an Untrained Model to the Data in order to adjust the weights,  
586 hyperparameters and/or structure thereof.

587 (i) *Trained Model* means a Model that is exposed to Data such that its weights, parameters  
588 and architecture embody insights from the Data.

589 (j) *Untrained Model* means Model that is conceived and reduced to practice as to its  
590 structure, components and architecture but that has not been trained on Data such that  
591 its weights, parameters and architecture do not embody insights from the Data.

592 **2. General Clauses**

593 (a) Unless otherwise agreed in writing by the parties, the data is licensed as is and as  
594 available. Lessor excludes all representations, warranties, obligations, and liabilities,  
595 whether express or implied, to the maximum extent permitted by law.

596 (b) Nothing in this License permits Licensee to make use of Lessors trademarks,  
597 tradenames, logos or to otherwise suggest endorsement or misrepresent the relationship  
598 between the parties.

599 (c) The rights granted under this license are deemed to be non-exclusive, worldwide,  
600 perpetual and irrevocable, unless otherwise specified in writing by Lessor.

601 (d) Without limiting Licensees rights available under applicable law, all rights not expressly  
602 granted hereunder are hereby reserved by Lessor. The Data and the database under  
603 which it is made available remain the property of Lessor (and/or its affiliates or  
604 licensors).

605 (e) This license shall be terminated upon any breach by Licensee of the terms of this  
606 License.

607 **3. Licensed Rights to the Data**

608 (a) Licensor hereby grants the following rights to Licensee with respect to making use of  
609 the Data itself.

- 610 i. Access the Data, where access means to access, view and/or download the Data to  
611 view it and evaluate it (evaluation algorithms may be exposed to it, but no Untrained  
612 Models).
- 613 ii. Creation of Tagged Data.
- 614 iii. Distribute the Data, i.e. to make all or part of the Data available to Third Parties  
615 under the same terms as those of this License.
- 616 iv. Creation of a Representation of the Data.

617 **4. Licensed Rights in Conjunction with Models**

618 (a) Licensor hereby **grants** the following rights to Licensee with respect to making use of  
619 the Data in conjunction with Models.

- 620 i. *Benchmark*: To access the Data, use the Data as training data to evaluate the  
621 efficiency of different Untrained Models, algorithms and structures, but excludes  
622 reuse of the Trained Model, except to show the results of the Training. This includes  
623 the right to use the dataset to measure performance of a Trained or Un-trained  
624 Model, without however having the right to carry-over weights, code or architecture  
625 or implement any modifications resulting from the Evaluation.
- 626 ii. *Research*: To access the Data, use the Data to create or improve Models, but  
627 with-out the right to use the Output or resulting Trained Model for any purpose  
628 other than evaluating the Model Research under the same terms.
- 629 iii. *Publish*: To make available to Third Parties the Models resulting from Research,  
630 provided however that third parties accessing such Trained Models have the right  
631 to use them for Research or Publication only.
- 632 iv. *Internal Use*: To access the Data, use the Data to create or improve Models and  
633 resulting Output, but without the right to Output Commercialization or Model  
634 Commercialization. The Output can be used internally for any purpose, but not  
635 made available to Third Parties or for their benefit.

636 (b) The rights granted in (a) above **exclude** the following rights with respect to making use  
637 of the Data in conjunction with Models:

- 638 i. *Output Commercialization*: To access the Data, use the Data to create or improve  
639 Models and resulting Output, with the right to make the Output available to Third  
640 Parties or to use it for their benefit, without the right to Model Commercialization.
- 641 ii. *Model Commercialization*: Make a Trained Model itself available to a Third Party,  
642 or embodying the Trained Model in a product or service, with or without direct  
643 access to the Output for such Third Party.

644 **5. Attribution and Notice Attribution and Notice**

645 The origin of the Data and notices included with the Data shall be made available to Third  
646 Parties to whom the Data, Output and/Model have been made available. Any distribution of  
647 all or part of the Data shall be done under the same terms as those of this License. Licensee  
648 shall make commercially reasonable efforts to link to the source of the Data. If so indicated  
649 by the Licensor in writing alongside the Data that the use shall be deemed confidential, then  
650 Licensee shall not publicly refer to Licensor and/or the source of the Data.

### A.9.1 Motivation

*For what purpose was the dataset created? Was there a specific task in mind? Was there a specific gap that needed to be filled? Please provide a description.*

This dataset was created to provide images of different types of Canadian croplands to study cropland classification using geo-referenced and multitemporal data. This dataset was created to help improve the classification of Canadian croplands using remote sensing imagery under multiple possible scenarios (in a temporal and/or static image classification context).

*Who created the dataset (e.g., which team, research group) and on behalf of which entity (e.g., company, institution, organization)?*

The dataset was created in 2021 by a research scientist (Dr. Etienne Lord), a doctoral student (Amanda A. Boatswain Jacques) of Agriculture and Agri-Food Canada (AAFC), and a professor at the University of Quebec in Montreal (UQAM) (Dr. Abdoulaye Baniré Diallo).

*Who funded the creation of the dataset? If there is an associated grant, please provide the name of the grant or and the grant number.*

The construction of this dataset was funded by AAFC, the department of the Government of Canada that is responsible for policies governing agricultural production, processing and marketing of all farm, food and agri-based products. This project is associated with the Smart Land Management Approach Grant. This project was also funded by a UQAM internal grant.

*Any other comments?* N/A.

### A.9.2 Composition

*What do the instances that comprise the dataset represent (e.g., documents, photos, people, countries)? Are there multiple types of instances (e.g., movies, users, and ratings; people and interactions between them; nodes and edges)? Please provide a description.*

The instances that comprise this dataset are satellite images of Canadian croplands that are sorted according to crop type, location throughout the country and date.

*How many instances are there in total (of each type, if appropriate)?*

The cleaned dataset contains a total of 78,536 distinct instances from 10 predominant crop types. The number of instances per class is reported below:

Crop types	Instances
CORN	12878
CANOLA	11366
PASTURE	8797
SPRING WHEAT	8229
ORCHARD	6594
BARLEY	5382
POTATO	5294
MIXEDWOOD	4981
OAT	4807
<b>TOTAL</b>	<b>78536</b>

The raw version of the dataset may have up to 46 classes per year.

*Does the dataset contain all possible instances or is it a sample (not necessarily random) of instances from a larger set? If the dataset is a sample, then what is the larger set? Is the sample representative of the larger set (e.g., geographic coverage)? If so, please describe how this representativeness was validated and verified. If it is not representative of the larger set, please describe why not (e.g., to cover a more diverse range of instances, because instances were withheld or unavailable).*

The dataset is a sample of the different crop types within different months and year. However, the current dataset is captured in rolling manner.

*What data does each instance consist of? "Raw" data (e.g., unprocessed text or images) or features? In either case, please provide a description.*

Each instance of this dataset consists of a Sentinel-2 satellite image for a single geographical point taken at a specific time period. These images were scraped using the open-source geospatial analysis tool Google Earth Engine (GEE). Each image is composed of 12 spectral bands which range from the Visible (VNIR) and Near Infra-Red (NIR) to the Short Wave Infra-Red (SWIR) wavelengths. Each point corresponds to the center of a Canadian agricultural field of a specific crop type. The images represent an area of 640 x 640 m, captured at a resolution of 10 m/pixel.

***Is there a label or target associated with each instance? If so, please provide a description.***

Each instance is associated with a label that dictates the type of crop present within the image. This label is present in the filename of the instance. For example, *POINT\_2\_201909\_AB\_BARLEY* corresponds to the geographical location with a point ID of 2, was retrieved in September 2019 from the province of Alberta (AB), and belongs to the crop class BARLEY.

***Is any information missing from individual instances? If so, please provide a description, explaining why this information is missing (e.g., because it was unavailable).***

To the best of our knowledge, we think that the information for individual instances is completed.

***Are relationships between individual instances made explicit (e.g., users' movie ratings, social network links)? If so, please describe how these relationships are made explicit.***

There are no relationships between instances that are from distinct geographical locations. However, the label of two different instances originating from the same point I.D may change over time because of crop rotation.

***Are there recommended data splits (e.g., training, development/validation, testing)? If so, please provide a description of these splits, explaining the rationale behind them.***

The procured dataset already comes packaged in suggested yearly train/validation/test splits, where instances belonging to one split are not present in another split. Images mapping to the same geographical coordinates are kept together during the splitting process. The dataset is partitioned in such a way that 70% of the images of each crop category are reserved for training, 15% for validation and 15% for testing. However, it is also possible to combine data from multiple years and recreate unique sets that are favorable to user's needs using the accompanying python toolbox.

***Are there any errors, sources of noise, or redundancies in the dataset? If so, please provide a description.***

Each image corresponds to a single geographical point taken at varying time periods. Therefore, there is a degree of redundancy in this dataset useful to replicate cases. However, all

individual instances are unique. Some images may be affected by small remnants of clouds or discoloration. However, instances with significant noise levels were removed from the cleaned set.

***Is the dataset self-contained, or does it link to or otherwise rely on external resources (e.g., websites, tweets, other datasets)? Please provide descriptions of all external resources and any restrictions associated with them, as well as links or other access points, as appropriate.***

Yes, the dataset is fully self-contained. There are no restrictions associated with the images, and anyone can access the dataset through the provided link. A GitHub repository is also provided with benchmarking code and a README.md file to explain how to use and manipulate the dataset.

***Does the dataset contain data that might be considered confidential (e.g., data that is protected by legal privilege or by doctor-patient confidentiality, data that includes the content of individuals' non-public communications)?***

No, the dataset does not contain any confidential information. All image information is retrieved directly from Google Earth Engine and the Canadian Annual Crop Inventory which are both open-source.

***Does the dataset contain data that, if viewed directly, might be offensive, insulting, threatening, or might otherwise cause anxiety?***

No.

***Any other comments?*** N/A.

### A.9.3 Collection Process

***How was the data associated with each instance acquired? Was the data directly observable (e.g., raw text, movie ratings), reported by subjects (e.g., survey responses), or indirectly inferred/derived from other data (e.g., part-of-speech tags, model-based guesses for age or language)? If data was reported by subjects or indirectly inferred/derived from other data, was the data validated/verified? If so, please describe how.***

A total of 6,633 geographical points corresponding to agricultural fields in Canada were randomly selected using Google Earth Engine. The images were webscraped directly from GEE. The label associated with each field

was retrieved using the ACI for that specific year (2017-2020, as of June 9th, 2022). The data was verified using manual observation to exclude any image samples that were deemed low quality.

**What mechanisms or procedures were used to collect the data (e.g., hardware apparatus or sensor, manual human curation, software program, software API)? How were these mechanisms or procedures validated?**

A python script was created to access the GEE application programming interface (API) and download all the available Sentinel-2 satellite band images per point. If there was no imagery available (due to high cloud or shadow cover post filtering), no imagery was downloaded.

**If the dataset is a sample from a larger set, what was the sampling strategy (e.g., deterministic, probabilistic with specific sampling probabilities)?**

The dataset represents a fraction of the full ACI. The subset was created by randomly manually tagging points using the 2019 and 2020 ACI, and GEE. Following this, imagery from previous years was extracted from these same points (when available) automatically.

**Who was involved in the data collection process (e.g., students, crowdworkers, contractors) and how were they compensated (e.g., how much were crowdworkers paid)?**

Two individuals were involved in the data collection process. These include a PhD student and a research scientist at AAFC. The student was paid as a part-time intern while the research assistant was paid as a full-time employee .

**Over what time frame was the data collected? Does this time frame match the creation time frame of the data associated with the instances (e.g., recent crawl of old news articles)? If not, please describe the time frame in which the data associated with the instances was created.**

The points were collected during the period of mid-march 2021 to mid-april 2021 and January 2022 to March 2022. This time frame does not match the time frame when the data was created (June 2017 - October 2019).

**Were any ethical review processes conducted (e.g., by an institutional review board)? If so, please provide a description of these review processes, including the outcomes, as well as**

**a link or other access points to any supporting documentation.** No.

**Does the dataset relate to people? If not, you may skip the remainder of the questions in this section.** No.

**Any other comments?** N/A.

#### A.9.4 Preprocessing / Cleaning / Labeling

**Was any preprocessing/cleaning/labeling of the data done (e.g., discretization or bucketing, tokenization, part-of-speech tagging, SIFT feature extraction, removal of instances, processing of missing values)? If so, please provide a description. If not, you may skip the remainder of the questions in this section.**

The data was preprocessed by generating sets of images based on the 12 bands retrieved from Sentinel-2. These sets correspond to RGB images, as well as commonly used vegetation indices. These processed images are in .png format and are in their respective sets (RGB, GNDVI, NDVI, NDVI45, OSAVI, PSRI). A color correction algorithm was applied to the RGB dataset.

Once the images were scraped from the satellite database, a program was created to preprocess the dataset and remove the images with too much cloud, shadows or missing data. This was done using the RGB images. If an image had any cloudy region over the field area, it was automatically removed from the dataset.

**Was the “raw” data saved in addition to the preprocessed/cleaned/labeled data (e.g., to support unanticipated future uses)? If so, please provide a link or other access point to the “raw” data.**

Yes. The raw dataset for each point is available as a .zip file where all the spectral bands and composite bands are saved in a .tiff format. The raw dataset can be accessed using the GitHub or Google Drive links indicated above.

**Is the software used to preprocess /clean/label the instances available? If so, please provide a link or other access point.** No.

**Any other comments?** N/A.

#### A.9.5 Uses

**Has the dataset been used for any tasks already? If so, please provide a description.**

To date, the dataset has been used solely for research tasks. Benchmarking tests were performed in the summer of 2021 at the 42nd Canadian Symposium of Remote Sensing, and for the 2021 NeurIPS Datasets and Benchmarks Track.

***Is there a repository that links to any or all papers or systems that use the dataset? If so, please provide a link or other access point.***

No, there is no existing repository for papers or systems using this dataset.

***What (other) tasks could the dataset be used for?***

Following the definitions of the Montreal Data License, the dataset can be used for benchmarking (training of models and evaluation of results), research, publishing (models resulting from research) and internal use. The dataset may NOT be used for output commercialization and/or model commercialization. The dataset was created primarily for image classification tasks, but can also be used for data augmentation and the generation of missing images in crop analyses.

***Is there anything about the composition of the dataset or the way it was collected and preprocessed/cleaned/labeled that might impact future uses? For example, is there anything that a future user might need to know to avoid uses that could result in unfair treatment of individuals or groups (e.g., stereotyping, quality of service issues) or other undesirable harms (e.g., financial harms, legal risks)? If so, please provide a description. Is there anything a future user could do to mitigate these undesirable harms?***

Expansion of the dataset is limited by the availability of Google Earth Engine. However, as it is released now, there are no limitations to the dataset.

***Are there tasks for which the dataset should not be used? If so, please provide a description.*** No.

***Any other comments?*** N/A.

#### A.9.6 Distribution

***Will the dataset be distributed to third parties outside of the entity (e.g., company, institution, organization) on behalf of which the dataset was created? If so, please provide a description.***

Yes, the dataset will be distributed by the University of Quebec in Montreal. It will be distributed to third parties.

***How will the dataset be distributed (e.g., tarball on website, API, GitHub)? Does the dataset have a digital object identifier (DOI)?***

The dataset will be distributed via a website hosted at the University of Quebec in Montreal. A GitHub repository with data manipulation tools and machine learning code for the benchmarking tests are available as well.

***When will the dataset be distributed?***

The dataset is currently available for download via the links provided in section A.9.2.

***Will the dataset be distributed under a copyright or other intellectual property (IP) license, and/or under applicable terms of use (ToU)? If so, please describe this license and/or ToU, and provide a link or other access point to, or otherwise reproduce, any relevant licensing terms or ToU, as well as any fees associated with these restrictions.***

The dataset is distributed under the Montreal Data License (see Appendix A.8).

***Have any third parties imposed IP-based or other restrictions on the data associated with the instances? If so, please describe these restrictions, and provide a link or other access point to, or otherwise reproduce, any relevant licensing terms, as well as any fees associated with these restrictions.*** No.

***Do any export controls or other regulatory restrictions apply to the dataset or to individual instances? If so, please describe these restrictions, and provide a link or other access point to, or otherwise reproduce, any supporting documentation.*** No.

***Any other comments?*** N/A.

#### A.9.7 Maintenance

***Who is supporting/hosting/maintaining the dataset?***

The University of Quebec in Montreal Bioinformatics laboratory will be hosting the dataset, but it will be continuously maintained by University of Quebec in Montreal and Agriculture and Agrifood Canada.

***How can the owner/curator/manager of the dataset be contacted (e.g., email address)?***

To inquire about this dataset, please email  
boatswain\_jacques.amanda@courrier.  
uqam.ca.

*Is there an erratum? If so, please provide a link  
or other access point.*

There is no erratum at this point.

*Will the dataset be updated (e.g., to correct  
labeling errors, add new instances, delete  
instances)? If so, please describe how often, by  
whom, and how updates will be communicated  
to users (e.g., mailing list, GitHub)?*

Yes, the dataset will be updated at least yearly when the annual crop inventory is available, to retrieve new images and crop labels. There is also the possibility to expand the dataset through the collection of additional points within Canada.